JOURNAL OF CATALYSIS 126, 147–172 (1990)

One- and Two-Component Diffusion in Zeolite ZSM-5

II. Experimental

WAQAR R. QURESHI[1] AND JAMES WEI

Department of Chemical Engineering, Massachusetts Institute of Technology, Cambridge, Massachusetts 02139

Received October 4, 1989; revised March 26, 1990

Counterdiffusion and codiffusion for benzene and toluene in ZSM-5 have been measured systematically to examine the effects of the occupancies of the diffusing components. These results are in good agreement with a theoretical model of single-file diffusion.

The one-component diffusion coefficients were essentially independent of occupancy up to occupancies of about 0.75. Codiffusion experimental results show apparent diffusivities of similar magnitude to one-component diffusivities, and almost independent of occupancies. The counterdiffusion experimental data show greatly reduced apparent diffusion coefficients, which are functions of the occupancies of the two components.

The diffusion trends with occupancy for all the diffusivities (one-component, counterdiffusion, and codiffusion) were very similar for the two ZSM-5 samples studied, even though these samples had very different Si/Al ratios (110 and 6000) and morphologies. The absolute values of the diffusivities, though, were a factor of 3 higher in the material with the higher Si/Al ratio. The sorption behavior was essentially identical for the two materials.

INTRODUCTION

A most interesting aspect of catalysis by ZSM-5 is molecular shape selectivity, which originates from configurational diffusion effects, and from steric inhibition of site kinetics (*1*). The usefulness of ZSM-5 arises from its pore dimensions, of about 5.5 Å in diameter, which are comparable to the molecular size of species like benzene, toluene, and xylenes.

There is, thus, a need to understand the diffusive behavior of molecules in ZSM-5 and other zeolites. Several different types of diffusion coefficients may be measured. Counterdiffusion and codiffusion are probably two of the most interesting measurements that can be made. Counterdiffusion occurs in chemical reactions, since feed molecules diffuse into the catalyst as the product molecules are diffusing out. Codiffusion occurs in adsorption separations when two or more species competitively adsorb into the molecular sieves. In addition, the study of counterdiffusion and codiffusion can improve the fundamental understanding of the configurational diffusion regime.

This paper describes experimental data for the counterdiffusion and codiffusion of benzene and toluene in ZSM-5, and compares them with predictions from a theoretical model. The details of this model and further theoretical considerations have been given by Qureshi and Wei (*2*).

In addition, we have also investigated the effect of Si/Al ratio and morphology on both one- and two-component diffusion. This part of the study was performed because considerable variation has been reported in the diffusivities obtained on different ZSM-5 crystals. Our aim here was not only to explore the effect of Si/Al ratio and morphology, but to also determine if there are some consistent trends in diffu-

[1] Present address: Chevron Research and Technology Company, Richmond, CA 94802.

0021-9517/90 $3.00

sion coefficients that are independent of the particular crystals used.

One-Component Diffusion in ZSM-5

Sorption uptake has been the most common method for measuring rates of diffusion in ZSM-5 (*3–13*). Other methods used include chromatography (*14, 15*), Wicke–Kallenbach (*16*), reaction diffusivity (*17, 18*), frequency response (*5*), NMR (*19, 20*), sorption/desorption technique (*21*), and zero-length column method (*22*).

Multicomponent Diffusion in Zeolites

To date, not very much work has been done on counterdiffusion, or on codiffusion in zeolites. Habgood (*23*) studied the sorption of nitrogen, methane, and their mixtures in Zeolite 4A. These were codiffusion experiments, and occupancy effects were not considered explicitly. The phenomena of displacement was observed, with the more weakly adsorbed but faster diffusing component being displaced by the more strongly adsorbed but slower diffusing component. Riekert (*24*) conducted experiments on the counterdiffusion of ethane and carbon dioxide in zeolite HT, and found a reduction in diffusivity of about an order of magnitude compared to one-component sorption. Ma and Roux (*25*) studied the binary diffusion of sulfur dioxide and carbon dioxide in sodium mordenite pellets. Their results showed that the apparent diffusivity of sulfur dioxide, when counterdiffusing into a system containing carbon dioxide, was between 20 and 50% lower than for uptake into a system that contained only the helium carrier gas. The codiffusion of benzene and *n*-heptane into Na–X Zeolite has been studied by Kärger and Bülow (*26*). They also observed the displacement phenomena, as did Ma and Lee (*27*), who studied binary gas phase mixtures in Zeolite X pellets, and found that in two-component uptake codiffusion experiments the diffusion coefficients were about an order of magnitude lower than for one-component uptake experiments.

Ruthven and Kumar (*28*), and Kumer *et al.* (*29*) used the chromatographic technique to study binary mixtures in A type zeolites. They found that their results were consistent with the hypothesis that each species in the mixture diffuses independently with the same intrinsic mobility as for single-component diffusion at the same temperature.

Yasuda and Matsumoto (*30*) used the frequency response method to determine diffusivities in a two-component N_2–O_2 mixture adsorbed in 4A zeolite. The highest total occupancy studied corresponded to 0.0232 molecules per cage. However, even at this low occupancy, considerable interactions were observed.

Liquid counterdiffusion has been studied by Satterfield and Katzer (*31*), and Satterfield and Cheng (*32*). An important result of these studies was that counterdiffusion in a binary system was much slower than adsorption in a single-component system.

Multicomponent Diffusion in ZSM-5

The multicomponent diffusion studies performed on zeolite ZSM-5 specifically have been limited so far to cases where one component can be considered to be stationary, relative to the high mobility of a second component. Nayak and Riekert (*8*) studied the uptake of benzene or toluene in ZSM-5 that contained previously adsorbed pyridine. Förste *et al.* (*33*) utilized NMR methods to study the molecular mobility of methane as a function of coadsorbed benzene. The much slower moving benzene molecules were assumed to be stationary relative to the more mobile methane molecules. They utilized the stochastic model of Theodorou and Wei (*34*) to analyze their diffusion results. One of the major conclusions from this work was that the benzene molecules reside at the channel intersections rather than in the channel segments. This conclusion was supported by the laser-Raman spectra and proton magnetic resonance of benzene adsorbed in ZSM-5. Kärger *et al.* (*35*) also used NMR tech-

TABLE 1

Diffusion Coefficients (10^{-10} cm^2 s^{-1}) for Benzene in ZSM-5 Measured by either the Gravimetric or Volumetric Uptake Methods

Reference	Method	Zeolite	Si/Al	Temp. (°C)	D	D^a at 65°C
(*3*)	grav.	Silicalite	—	50	1[b]	1
(*3*)	grav.	HZSM-5	90	50	1[b]	1
(*4*)	vol.	Na, HZSM-5	135	60	7[b]	8
(*4*)	grav.	Na, HZSM-5	135	60	4[b]	5
(*4*)	grav.	Silicalite	>1000	60	20[b]	20
(*6*)	grav.	HZSM-5	150	90	4[c]	2
(*7*)	grav.	HZSM-5	23	28	0.066[d]	0.2
(*8*)	grav.	HZSM-5	20 to 50	25	0.06	0.2
(*11*)	grav.	Silicalite	—	20	0.086	0.3
(*12*)	grav.	HZSM-5	17	40	2.5	5

[a] Data extrapolated to 65°C, assuming an activation energy of 24 kJ mol^{-1}.
[b] Diffusivity at about 0.3 molecules per intersection, recalculated from the published corrected diffusivity.
[c] At about 0.3 molecules per intersection.
[d] Assuming spherical particles.

niques to study the effect of coke deposition on the diffusion of probe molecules in ZSM-5. They were able to draw some conclusions of where coke deposition occurs from different source molecules. Mo (*36*) has looked at the effect of MgO blockages on the diffusion of aromatics in ZSM-5.

Choudhary *et al.* (*37*) have reported uptake data for liquid phase multicomponent systems in ZSM-5. The results are interpreted in terms of sorption rates, but the driving force for uptake has not been considered, and no diffusion coefficients are given.

The Effect of Si/Al Ratio and Morphology

Single component diffusion data reported in the literature cover a range of several orders of magnitude. Table 1 is a partial list of data that has been taken using either a gravimetric or a volumetric uptake method (*3, 4, 6–8, 11, 12*). We have brought the diffusivities to a common temperature basis of 65°C in the last column of the table by assuming an activation energy of 24 kJ mol^{-1}. The differences in measured diffusion coefficients could have arisen from variations in crystal composition, structure, and morphology, as well as from the choice of the characteristic diffusion length.

The effect of Si/Al ratio has been studied by Zikanova *et al.* (*4*), who, using a gravimetric method, found that for the diffusion of benzene in Na, HZSM-5, the diffusion coefficient was a half order of magnitude higher for a material with Si/Al > 1000 than it was for a material with Si/Al = 135. Post *et al.* (*38*), utilizing a chromatographic method, found an increase in the diffusivity of 2,2 dimethylbutane with increasing Si/Al ratio in a study of fifteen HZSM-5 samples ranging in Si/Al ratio from 24 to 7000. The overall increase was about a factor of 1.6. Choudhary and Srinivasan (*21*) employed a dynamic sorption/desorption technique, and found that the diffusivity of benzene in HZSM-5 increased with increase in Si/Al ratio. In contrast with these results Caro *et al.* (*19*), using the NMR technique, found no substantial influence of the Si/Al ratio on the diffusivity of methane in HZSM-5 and Na,HZSM-5 for Si/Al ratios ranging from 40 to greater than 1000.

Sorption may also be influenced by Si/Al ratio or cation exchange. For instance,

Choudhary and Srinivasan (*21*), and Lechert and Schweitzer (*39*) found that sorption increases with a decrease in Si/Al ratio.

There is a reasonably consistent pattern in these results; that is, with the exception of the data of Caro *et al.* (*19*), we can say that aluminum decreases diffusivity and increases sorption.

Sorption and diffusion may also be influenced by cation exchange. For example, Wu and Ma (*40*) found a decrease in adsorption capacity with increasing cation radius, but no significant effect of the cation on diffusion rates. Forni *et al.* (*14*) observed that for benzene and methyl benzenes, HZSM-5 showed a much lower adsorption equilibrium constant and more rapid diffusion kinetics than the sodium form. Choudhary and Srinivasan (*21*) also found that benzene diffuses at a higher rate in the hydrogen form of ZSM-5 than it does in the sodium form.

With these variations in diffusivity being reported for one-component systems, the question arises as to what kind of variations could be expected in two-component systems. Also, even if the apparent diffusivity is found to vary significantly, can we at least find trends, both for one- and two-component systems, that are independent of crystal origin?

To answer these questions we have also conducted an investigation into the effect of Si/Al ratio and morphology on one- and two-component diffusion. We did this by comparing the results obtained on two samples of ZSM-5 which had different Si/Al ratios and morphologies.

METHODS

Characterization of ZSM-5 Samples

Two different ZSM-5 samples were used in this study. The first (Sample A) was supplied to us in the hydrogen form by Peter A. Jacobs of the Katholieke Universiteit, Leuven. The second sample (Sample B) was specially synthesized as described later. Both samples were analyzed for aluminum content. They were also characterized by powder X-ray diffraction, with both samples showing powder patterns that compared closely with the simulated peaks given by von Ballmoos (*41*). Finally, the morphology and size of the ZSM-5 crystals were determined by scanning electron microscopy.

Sample A had a Si/Al ratio of 110 which corresponds to 0.22 Al atoms per intersection. In contrast Sample B had a Si/Al ratio of 6000 $\pm$ 1000 which corresponds to less than 0.004 Al atoms per intersection. Here, the aluminum was present only as an impurity, as no aluminum was added during the synthesis. ZSM-5 with aluminum content as low as this is sometimes known as silicalite.

Figures 1 and 2 show SEM photographs for Sample A and Sample B, respectively. Sample B consists of particles with clean edges and the typical ZSM-5 elongated hexagonal shape. Some twinning and intergrowth is evident. The dimensions are approximately 12 $\times$ 20 $\times$ 30 μm. Sample A displays more faulting, the particles are more spherical or cubical in shape, and the average diameter of about 12 μm is of length similar to the smallest dimension of Sample B.

Synthesis of Sample B

We developed a technique to synthesize large quantities of ZSM-5 suitable for diffusion studies. The aim was to be able to synthesize 50 to 100 g quantities of crystals with a minimum dimension of at least about 10 μm. Large batches of crystals means that many experiments of different kinds can be conducted on the same batch, thereby avoiding problems with variation between samples. Our approach was to modify the technique of von Ballmoos (*42*).

Initially, a solution of approximately 20% by weight of tetrapropylammonium hydroxide was made by reacting a solution of tetrapropylammonium bromide with excess

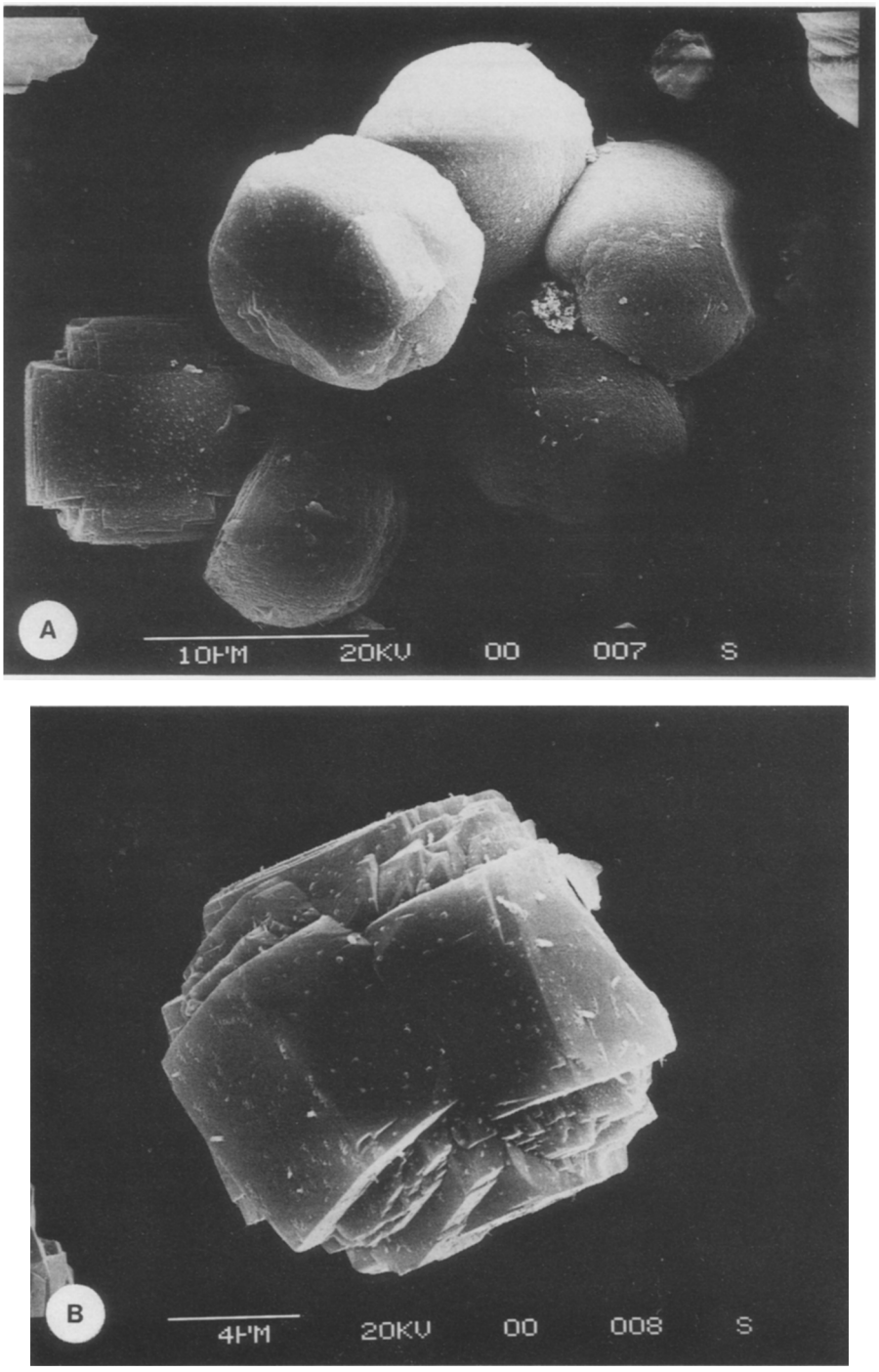

FIG. 1. Scanning electron micrographs of Sample A.

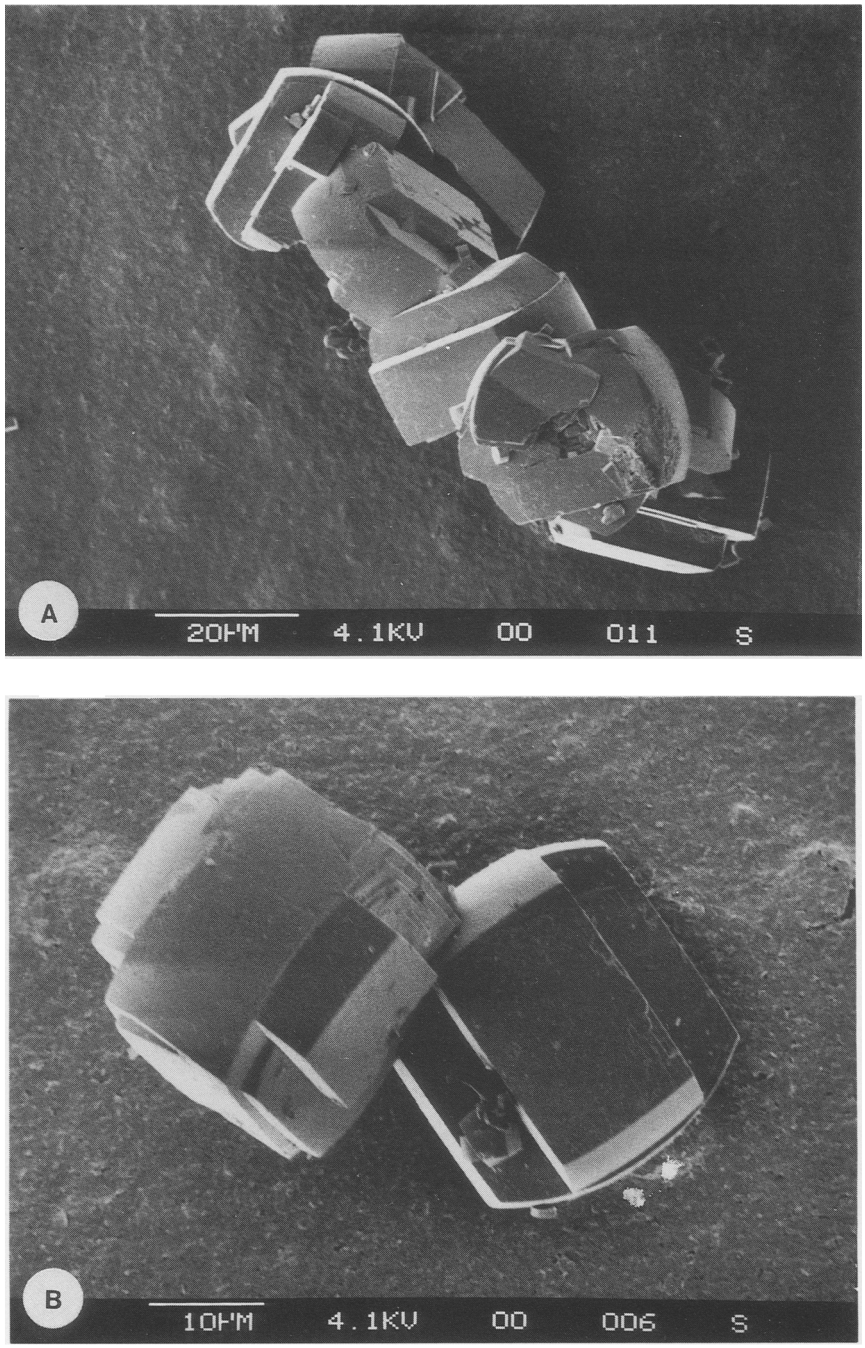

FIG. 2. Scanning electron micrographs of Sample B.

silver oxide, and by filtering out the resulting silver bromide precipitate.

The synthesis mixture for Sample B was made as follows: 94 g of silicic acid (Fluka 60780, puriss. p.a.) was placed in a polyethylene beaker. To this was added 209 ml of the tetrapropylammonium hydroxide solution, 288 ml of water, and 15 g of cesium chloride, and the mixture was stirred for about 1 h.

The resulting slurry was poured into a stainless steel liner, and placed in a 1-liter autoclave. The autoclave was sealed, purged with helium, and heated to 195°C at a rate of 1°C per min, with the stirring rate set to 50 rpm. These conditions were maintained for a period of 5 days, when the autoclave furnace was turned off, and the mixture allowed to cool to room temperature. The solid product was filtered and washed with ethanol and deionized water. Further details of the synthesis procedure are given by Qureshi (*43*).

The calcination stage was carried out in two steps. Approximately 5 g of the product was spread in a layer, approximately 1 mm thick, on a watch glass which was then placed in a muffle furnace. The furnace was purged with continously flowing nitrogen, and the temperature increased at a rate of 1 to 2°C per min up to 550°C. After approximately 12 h the furnace was turned off and allowed to cool to room temperature over a period of about 3 h. The flowing nitrogen was then turned off and the heating and cooling procedure repeated under air. This completed the synthesis procedure and the product could then be characterized as described above.

Multicomponent Diffusion Apparatus

Figure 3 shows a schematic of the multicomponent diffusion apparatus. It consists of a circulating system that includes a chamber for the catalyst bed. The circulating carrier gas consists of helium (Matheson, ultrahigh purity), with a bellows pump providing the circulation. An injection port is used to add small quantities of the component of interest, and a sampling valve

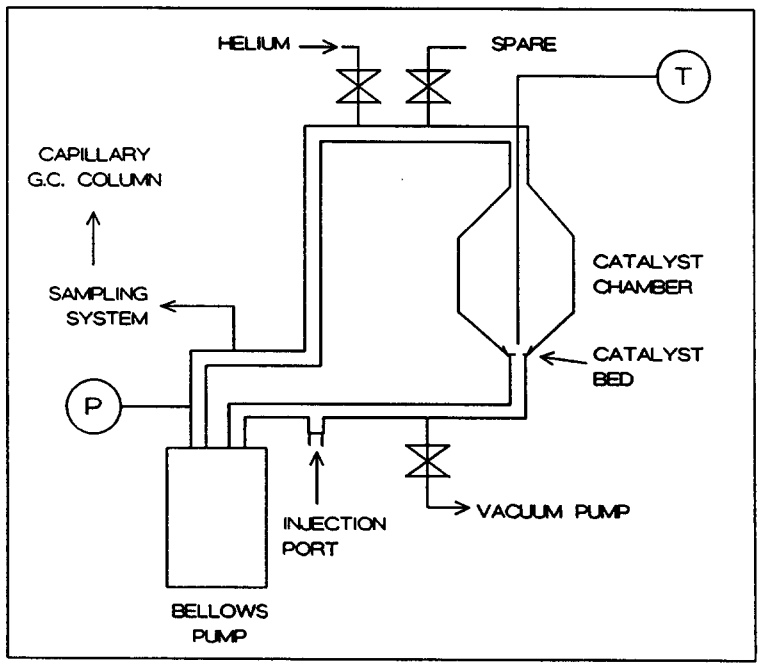

FIG. 3. The multicomponent diffusion apparatus designed and built for this study.

TABLE 2

Experimental Conditions

Volume of system	205 cm^3
Mass of catalyst	3 to 20 mg
Temperature	35 to 90°C
Total pressure (mostly He)	5 to 40 KPa
Hydrocarbon partial pressure	10 to 700 Pa
Area of catalyst bed	1 to 20 cm^2

system allows analyses to be performed by a gas chromatograph. The components studied were Benzene (Fluka 12545, high purity) and Toluene (Fluka 89678, high purity). A vacuum pump is used to evacuate the system and prepare it for experiments. The total pressure in the system is monitored by a capacitance pressure sensor. The catalyst chamber and attached tubing are made of glass; the other materials that come into contact with the circulating gases are stainless steel and teflon. Table 2 gives a summary of the range of conditions for the experiments conducted.

A fused silica capillary column was used in the gas chromatograph. This allowed analysis times as low as 30 s. Thus, if necessary samples could be taken as fast as two every minute. The metal bellows circulating pump has a capacity of 0.2 l/s when pumping against zero pressure head. The pump is completely contamination free as no lubrication is required.

Injections of the species of interest were made by microliter syringes, through a teflon backed septum. All injections were made in the liquid form. The amount injected varied between 0.25 and 2.5 μl. The injection port was kept heated to about 80°C to evaporate the sample quickly. In blank runs (no zeolite present) the first sample was taken within 5 s after making the injection. Complete evaporation and mixing had occurred within this time. A sequence of three multiport sampling valves were used. A somewhat complicated scheme was required, because it is necessary to take samples from a low pressure environment, and then inject them into the 400 kPa helium carrier gas going into the gas chromatograph. The vacuum pump is of the oil-sealed, rotary-vane type. It has a free air displacement rate of 0.8 l/s and an ultimate vacuum of 0.01 Pa. Figure 3 also shows the design of the catalyst chamber. A fine stainless steel mesh supports a small glass wool bed, in which the catalyst crystals (without pelletizing) were suspended. Heating tape and a proportional–integral-derivative temperature controller were used to maintain the temperature of the system. The thermocouple was placed to within 1 mm of the catalyst bed.

Any possible adsorption of the benzene or toluene onto the walls of the apparatus was minimized by:

1. Minimizing the stainless steel wall area—stainless steel adsorbs much more strongly than glass.
2. Silanizing all the internal glass surfaces.
3. Using teflon stopcock plugs, and a teflon-backed septum.
4. Using silanized chromatographic grade glass wool.
5. Cleaning the apparatus in an ultrasound bath with four different solvents, as described by Walker *et al.* (*44*).

The blank adsorption runs indicated that benzene diffusion measurements could be made at temperatures above 35°C, and toluene measurements could be made above 65°C. Below these temperatures adsorption on the apparatus walls could be significant.

There was no difference in measured pressure with and without the presence of the catalyst bed, indicating that there was no significant pressure drop across the bed. It follows from the bellows pump characteristics that there was one complete revolution of the circulating gases every second. The diffusion experiments took 600 s or longer to reach equilibrium. The time constant for circulation of 1 s is therefore much smaller than the time constants for the diffusion experiments, and so it was assumed that the system is well mixed.

Diffusion Experiments

At the beginning of each experiment the ZSM-5 was calcined at 525°C in a muffle furnace for 12 h under air. This was done to burn off any hydrocarbons which may have adsorbed on the crystals. The crystals were heated over a period of about 3h, and cooled over a period of about 2 h. Exposure to room air at room temperature was kept to a minimum. We observed that if exposure was as long as say 12 h, even in a capped bottle, the diffusion results could be significantly lower. It may be that significant amounts of hydrocarbons are adsorbed from the room air at low temperatures. The catalyst was weighed and then placed in the apparatus. The amount of catalyst used varied between 3 and 20 mg, depending on the sorbed component, and on which part of the isotherm the experiment was to be conducted. The apparatus was immediately evacuated by the vacuum pump, and heated to the experiment temperature. Helium was introduced at a pressure of about 13 kPa and the bellows circulation pump was switched on. Experiments were started after a period of about 1 h, during which time steady state was achieved. Injections were made into the apparatus with microliter syringes, and the gas phase concentrations were monitored by sampling to the gas chromatograph. Each sample consists of 0.1% of the system volume. Between 10 and 15 samples were taken for each uptake experiment. The experiments were conducted with relative pressures (P/P_{sat}) up to about 0.002. (P_{sat}, the saturated vapor pressure is 61.8 kPa for Benzene at 65°C, and 22.4 kPa for Toluene at 65°C.)

In preliminary one-component experiments, several variables were tested to see if they had an effect on the observed diffusion coefficients. It was found that the results were insensitive to the amount of helium present (varied from 5 to 40 kPa), the mass of catalyst used (varied by a factor of 3), the amount of toluene or benzene injected (varied by a factor of 2), and to the time period of calcination (varied from 8 to 24 h).

The fact that varying the helium pressure had no effect is not surprising, as its occupancy should be very low. This was confirmed by doing an approximate calculation that assumed that the concentration of the helium in the adsorbed phase was the same as in the gas phase. That is, it was assumed that helium behaves as a completely ideal gas. This gives an estimated occupancy of only 0.004 helium molecules per intersection at 65°C and 13 kPa.

For the one-component experiments, sequential injections of the sorbed component were made. The gas phase concentration was measured each time until equilibrium was reached. In the case of the counterdiffusion experiments, the first component was injected and the system allowed to attain equilibrium. The second component was then injected, and the gas phase concentration monitored to obtain the rates of desorption of the first component and sorption of the second component as functions of time. For the codiffusion experiments, both components were injected, and the system allowed to come to equilibrium. This initial injection was performed in such a manner that the two components attained equal occupancies in the catalyst when equilibrium was reached. Then the actual uptake experiment was performed, the components being injected in the same molar ratio as their gas phase concentrations. The gas phase concentrations were monitored after this second injection, so as to obtain the uptake curves for both components.

Analysis

The primary thrust of this paper is the comparison between the trends of the experimental and theoretical two-component results. The approach is to calculate "apparent diffusivities," as defined by Qureshi and Wei (*2*), for the two-component experimental results, and compare them with the

calculated results from the model of Tsikoyiannis (*6*).

To calculate the theoretical apparent diffusion coefficients, we first had to obtain the hopping rates q_1 and q_2 that would be used as input parameters for the two-component simulations. These hopping rates were obtained by fitting the model to one-component experimental results. For a one-component system, the model predicts the usual Fick's Diffusion Equation and Langmuir Isotherm boundary conditions. Thus, the one-component results were fitted to

$$\frac{\partial \theta}{\partial t} = D \nabla^2 \theta \tag{1}$$

with the boundary condition,

$$\theta = \frac{KP}{1 + KP}, \quad r = R, \tag{2}$$

initial condition,

$$\theta = \theta_0, \quad t = 0, \tag{3}$$

and mass balance between the gas and adsorbed phases,

$$\frac{V_g}{R_g T} \frac{\partial P}{\partial t} = -m\rho \frac{\partial \bar{\theta}}{\partial t} \tag{4}$$

In these equations P is the partial pressure of the component of interest. The balance of the gas phase consists of the helium carrier gas. Now from the model $D = \alpha^2 q$, where α is the distance between grid intersections (jump length), and so we can obtain $\alpha^2 q_1$ and $\alpha^2 q_2$ for the two components.

The next step is to use the model for two-component systems to simulate the two-component experiments. To do this, we use Eqs. (5)–(10) to generate the simulated "approach to equilibrium" curves (uptake or desorption curves),

$$\frac{\partial \underline{\theta}}{\partial t} = \nabla (\mathbf{D} \nabla \underline{\theta}), \tag{5}$$

where

$$\mathbf{D} = \alpha^2 \begin{bmatrix} q_1 & 0 \\ 0 & q_2 \end{bmatrix} \begin{bmatrix} (1 - \theta_2) & \theta_1 \\ \theta_2 & (1 - \theta_1) \end{bmatrix} \tag{6}$$

and

$$\underline{\theta} = \begin{bmatrix} \theta_1 \\ \theta_2 \end{bmatrix}. \tag{7}$$

The boundary conditions are of Langmuir form (which is the type of partitioning predicted by the theoretical model):

$$\theta_i = \frac{K_i P_i}{1 + K_1 P_1 + K_2 P_2}, \quad r = R, \; i = 1, 2. \tag{8}$$

The initial condition gives the initial loading in the catalyst:

$$\underline{\theta}_i = \underline{\theta}_{i0}, \quad t = 0, \; i = 1, 2. \tag{9}$$

Finally, there is a mass balance between the gas and adsorbed phases:

$$\frac{V_g}{R_g T} \frac{\partial P_i}{\partial t} = -m\rho \frac{\partial \bar{\theta}_i}{\partial t}, \quad i = 1, 2. \tag{10}$$

The boundary conditions, initial conditions, and mass balances were chosen to mimic experimental conditions, so that the theoretical simulations would be made with conditions that imitate the experimental conditions.

Now, to these simulated uptake or desorption curves we fit apparent diffusivities, $D_1^\dagger$, and $D_2^\dagger$, using

$$\frac{\partial \underline{\theta}}{\partial t} = \nabla(\mathbf{D}^\dagger \nabla \underline{\theta}), \tag{11}$$

where

$$\mathbf{D}^\dagger = \begin{bmatrix} D_1^\dagger & 0 \\ 0 & D_2^\dagger \end{bmatrix} \tag{12}$$

together with the boundary conditions, initial conditions, and mass balances of Eqs. (8)–(10).

The final step is to fit apparent diffusivities to the experimental approach to equilibrium curves. This is done in exactly the same way as the fitting of the apparent diffusivities to the simulated approach to equilibrium curves. That is, we use Eqs. (11) and (12), together with Eqs. (8)–(10). The only fitted parameters are $D_1^\dagger$ and $D_2^\dagger$. Thus, we have now calculated experimental apparent diffusivities and theoretical apparent

diffusivities in exactly the same way, and the results can be compared directly.

We report the one-component diffusivities and codiffusion apparent diffusivities at the average (total) occupancies in the crystals, where average occupancy is defined by (initial occupancy + final occupancy)/2. The counterdiffusion apparent diffusivities are reported at the average occupancy of the presorbed component.

In all of the above, the uptake and desorption curves were calculated using a finite element technique, and all of the fittings were performed using a least-squares regression method developed by Powell (*45*), and described by Kuester and Mize (*46*).

RESULTS AND DISCUSSION

One-Component Equilibrium

Figure 4 shows the single-component adsorption isotherms for benzene and toluene in both samples at 65°C. Also shown are fitted isotherms of the Langmuir form. The figure illustrates how toluene is adsorbed more strongly than benzene. The error bars in this and all other figures are representative of the estimated precision of the data. All concentrations in the adsorbed phase are expressed as occupancies. An occupancy of one (one molecule per intersection) corresponds to four molecules per unit cell, or about 6.93×10^{-4} mol g^{-1}.

There appears to be no significant difference in the adsorption properties of the two materials. The difference between the fitted curves never exceeds about 0.05 molecules per intersection, which could be accounted for by experimental error. This seems to indicate that the internal pore volume and structure in the two materials are quite similar. This is not surprising since the amount of aluminum in Sample A corresponds to 0.22 atoms per intersection, which may not cause a significant increase in adsorption properties when compared with Sample B which has about 0.004 aluminum atoms per intersection. Previous workers who found increased adsorption with aluminum content worked with larger aluminum concentrations. Choudhary and Srinivasan (*21*) worked with aluminum contents varying from 0.6 to 1.6 atoms per intersection, and Lechert and Schweitzer (*39*) had contents ranging from 0.5 to 2.2 atoms per intersec-

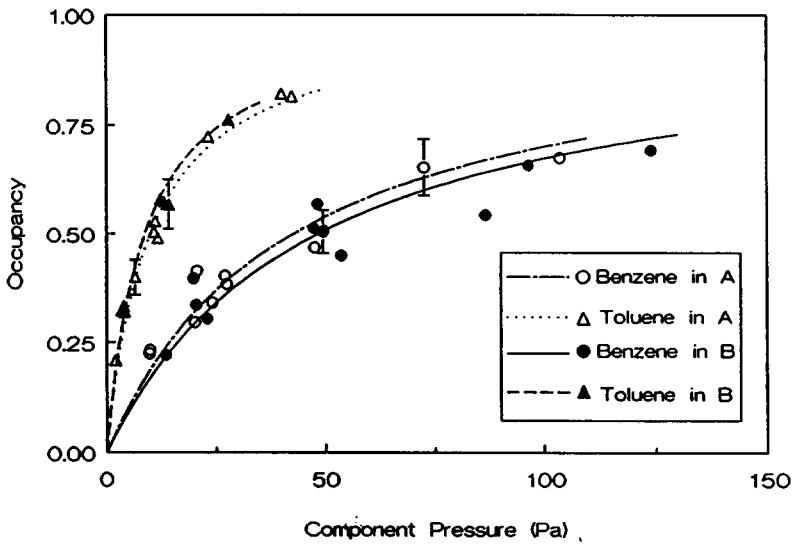

FIG. 4. Comparison of adsorption isotherms in Samples A and B at 65°C. The parameters for the fitted Langmuir Isotherms are $K_B = 0.024$ Pa^{-1} and $K_T = 0.10$ Pa^{-1} for Sample A, and $K_B = 0.021$ Pa^{-1} and $K_T = 0.12$ Pa^{-1} for Sample B.

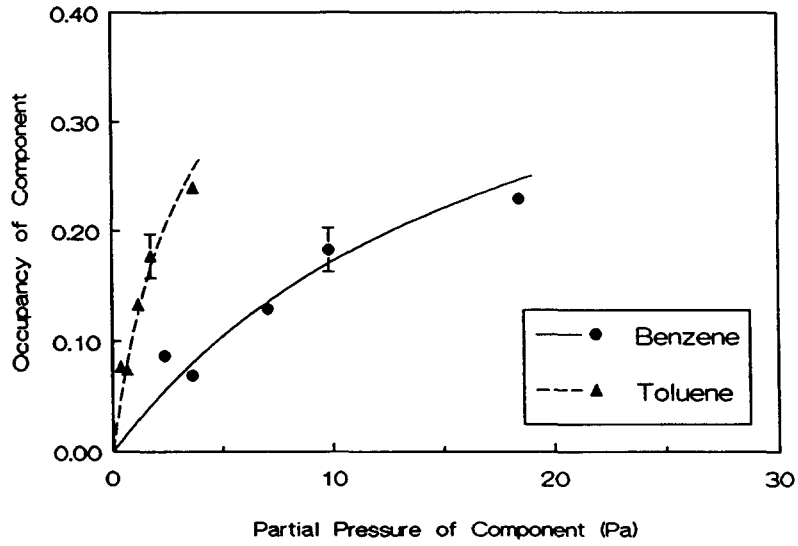

FIG. 5. Two-component equilibrium data in Sample A when the occupancies of benzene and toluene are equal, with fitted Langmuir Isotherms with the parameters $K_B = 0.025$ Pa^{-1} and $K_T = 0.14$ Pa^{-1}.

tion. Our results correspond well with those of Shah *et al.* (*3*) who observed that the isotherms for silicalite, containing essentially no aluminum, and a HZSM-5 with aluminum content of 0.26 atoms per intersection were virtually identical.

Figure 5 shows two-component data and fitted Langmuir Isotherms at 65°C for Sample A. In this figure, both components have occupancies that are equal to within 0.01 molecules per intersection. The partial pressure of each component, at this condition of equal occupancies, is shown on the abscissa, and the occupancy of each component is on the ordinate. The competitive adsorption effect is shown, with the toluene adsorbing more strongly than the benzene, resulting in the benzene requiring a larger partial pressure to attain the same occupancy as the toluene. This data was collected by injecting a mixture of benzene and toluene into the apparatus. The mixture composition was estimated beforehand so that at equilibrium both components would have equal occupancies.

Figure 6 gives the analogous results for Sample B. In this case, the experimental data includes only those points that satisfy the criterion that the occupancies of the two components are equal to within 0.03 molecules per unit cell.

Figure 7 verifies that for Sample A over the range of the two-component experiments conducted, we can approximate the equilibrium isotherms by a Langmuir form of Eq. (8). The figure gives a comparison of the two-component experimental data at 65°C with the theoretical results from a Langmuir Isotherm. This isotherm was fitted to the data and has the fitted parameters $K_B = 0.025$ Pa^{-1} and $K_T = 0.11$ Pa^{-1}. The data covers partial pressure ranges of 2 to 110 Pa for Benzene, and 0.4 to 16 Pa for Toluene. Clearly, over the range of pressures and occupancies studied, the Langmuir form describes the partitioning between the gas and the adsorbed phases reasonably well, and so it can serve to calculate the driving force for the diffusion measurements. The estimation of the boundary conditions for the diffusion measurements was further improved by using the Langmuir isotherm constants calculated for each particular experiment.

Figure 8 shows the two-component equilibrium data for Sample B at 65°C that was

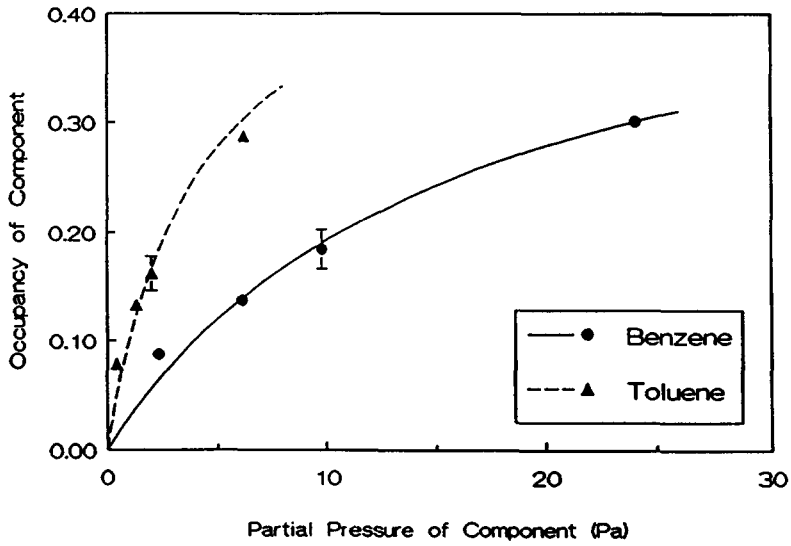

FIG. 6. Two-component equilibrium data in Sample B when the occupancies of benzene and toluene are equal, with fitted Langmuir Isotherms with the parameters $K_B = 0.032$ Pa^{-1} and $K_T = 0.12$ Pa^{-1}.

collected during the course of performing the diffusion experiments. The partial pressure ranges covered are 2 to 130 kPa for Benzene and 0.4 to 30 kPa for Toluene. This plot is analogous to Fig. 7, and shows the predicted occupancy from fitting a Langmuir isotherm against the experimentally observed occupancy. The fitted parameters are $K_B = 0.027$ Pa^{-1} and $K_T = 0.11$ Pa^{-1}. Once again, the Langmuir form is a reasonable model for the equilibrium behavior, and can serve to calculate the driving force for the diffusion measurements.

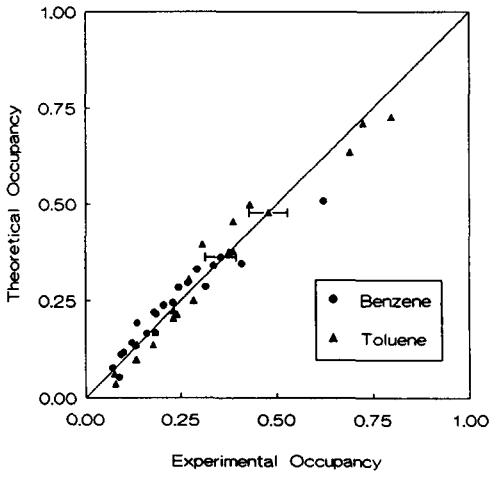

FIG. 7. Comparison between two-component equilibrium data and the predicted occupancies from a Langmuir Isotherm with the parameters $K_B = 0.025$ Pa^{-1} and $K_T = 0.11$ Pa^{-1} (Sample A).

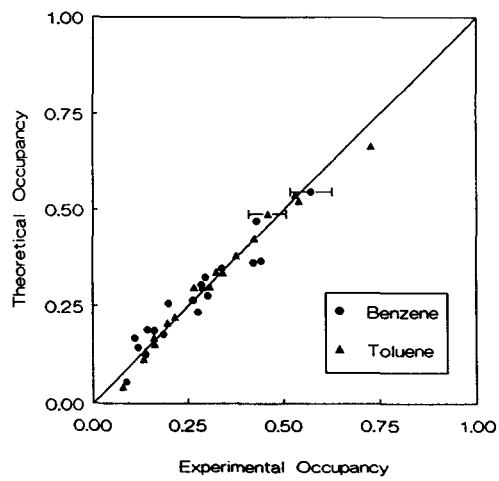

FIG. 8. Comparison between two-component equilibrium data and the predicted occupancies from a Langmuir Isotherm with the parameters $K_B = 0.027$ Pa^{-1} and $K_T = 0.11$ Pa^{-1} (Sample B).

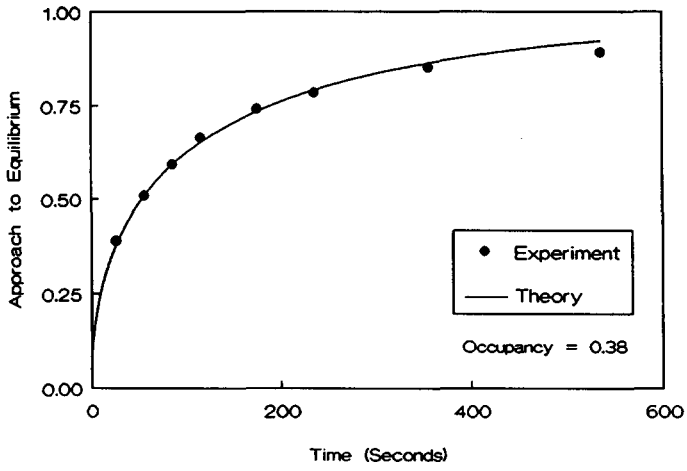

FIG. 9. Example of one-component uptake data in Sample A (Benzene at 65°C).

One-Component Diffusion

Figure 9 shows an example of one-component uptake with the fitted curve from Eqs. (1)–(4). There is only one fitted parameter, D, the one-component diffusivity.

Figure 10 shows one-component diffusion coefficients in Sample A for benzene at 90, 65, and 35°C. The measured activation energy is of the order of 24 kJ mol^{-1}, which compares closely with 28.8 kJ mol^{-1} obtained by Shah *et al.* (*3*), 26 and 18 kJ mol^{-1} by Zikanova *et al.* (*4*), and 21 kJ mol^{-1} by Wu *et al.* (*11*). All of these workers used a transient uptake method for diffusion measurement. It also compares closely with the 27 kJ mol^{-1} observed by Eic and Ruthven (*22*) who used the zero-length column method. The result of Choudhary and Srinivasan (*21*), using a sorption/desorption technique, is significantly higher at 64.4 kJ mol^{-1}.

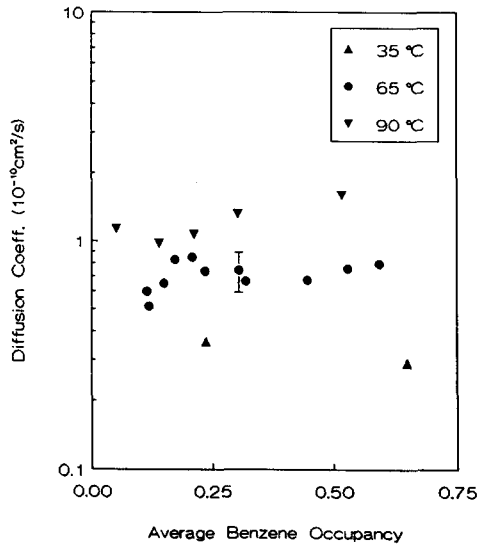

FIG. 10. Benzene diffusion coefficients in Sample A.

The results of Fig. 10 do not show any dramatic effect of occupancy on the diffusion coefficient, over the range of occupancies studied. This agrees with the results of Zikanova *et al.* (*4*), after they were converted back to the original uptake diffusion coefficients from the corrected diffusion coefficients presented in the paper. Tsikoyiannis (*6*) observed more strongly increasing trends with occupancy. Those results, however, were for different crystals, and extended to higher occupancies than the results reported in this study.

A temperature of 65°C was chosen to conduct the majority of the experiments. Figure 11 gives a summary of the one-component diffusion data for toluene and benzene in Sample A at this temperature. The toluene data lies in the range: 1 to 2 × 10^{-10} cm^2 s^{-1}; the benzene data is a little lower at

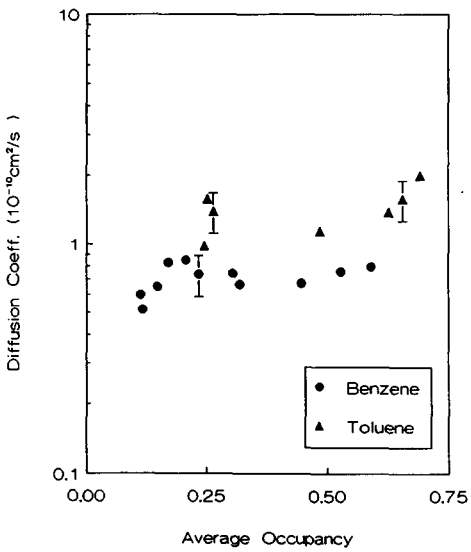

FIG. 11. One-component diffusivities of benzene and toluene in Sample A.

0.6 to 0.9 × 10^{-10} cm^2 s^{-1}. The ranges of these data agree reasonably well with the results previously reported by Shah *et al.* (*3*), Zikanova *et al.* (*4*), Tsikoyiannis (*6*), Doelle *et al.* (*12*), and Eic and Ruthven (*22*). The higher diffusivity of toluene is in agreement with Tsikoyiannis (*6*), but contrary to Nayak and Riekert (*8*).

Figure 12 shows single-component diffusivities for Sample B. At 65°C we obtain benzene diffusivities of 1.3 to 2.5 × 10^{-10} cm^2 s^{-1} and toluene diffusivities of about 2 to 4 × 10^{-10} cm^2 s^{-1}.

The results on Sample B are a factor of about 3 higher than the diffusivities obtained on Sample A. This trend agrees with the results of Zikanova *et al.* (*4*), Choudhary and Srinivasan (*21*), and Post *et al.* (*38*) who all found an increase in diffusivity with increasing Si/Al ratio.

The important point to note is that we see very similar trends in the diffusion coefficient with occupancy for the high (Sample B) and low (Sample A) Si/Al ratios studied. That is, there is not much change with occupancy, except for perhaps a slight increasing trend, which does not exceed a factor of about 2 over the complete range. Also, as in Sample A, toluene diffuses at a rate that is an average of about 50% higher than benzene.

Two-Component Diffusion

Figures 13 and 14 are examples of the calculations of the two-component apparent diffusivities. Figure 13 shows an example of the experimental results for the counterdiffusion of benzene and toluene in Sample A, with the toluene going into the catalyst and the benzene coming out. The fitted curves were obtained from Eqs. (8)–(12), with the only fitted parameters being the two apparent diffusivities, $D_1^\dagger$ and $D_2^\dagger$. Figure 14 shows an example of the calculation of apparent diffusivities for Sample A from the theoretical model. The simulated uptake and desorption curves are obtained from the model, that is, Eqs. (5)–(10). The input parameters for these simulations were $\alpha^2 q_B = 0.8 \times 10^{-10}$ cm^2 s^{-1} and $\alpha^2 q_T = 1.16 \times 10^{-10}$ cm^2 s^{-1}. These parameters were chosen to lie within the ranges of the one-component experimental data. The simulations, then, are the predictions from the model of the uptake and desorption curves for two-component diffusion, and can be

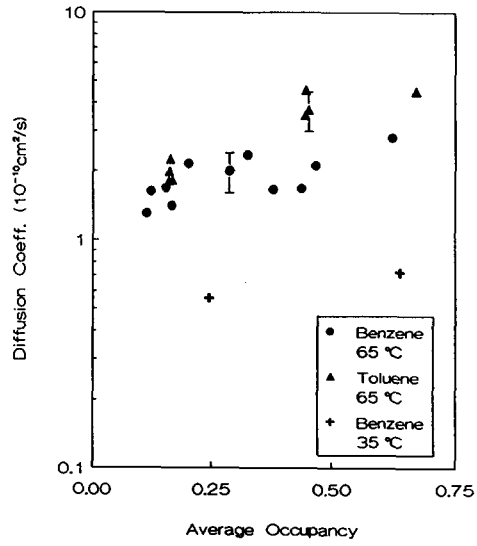

FIG. 12. One-component diffusivities of benzene and toluene in Sample B.

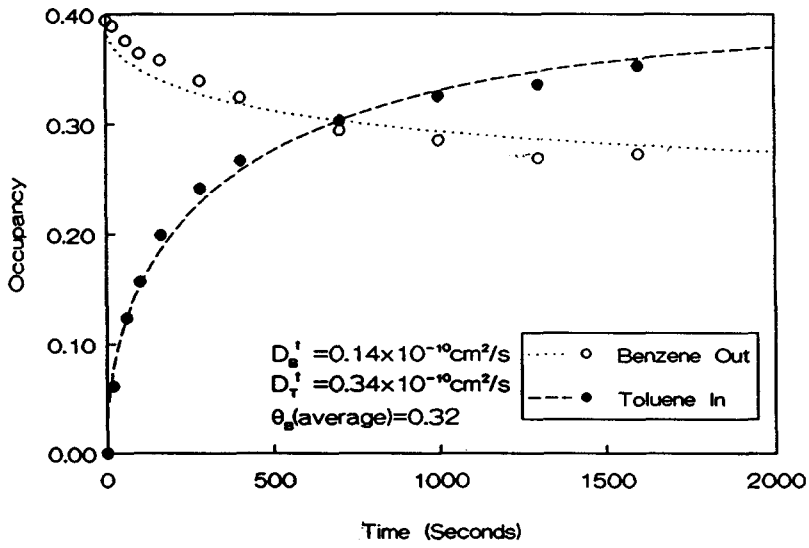

FIG. 13. Example of experimental counterdiffusion data in Sample A, together with the fitted curves that give the experimental apparent diffusivities.

compared with the two-component experimental results. This comparison is done by calculating the apparent diffusion coefficients, from these simulated uptake and desorption curves, in exactly the same way that the apparent diffusivities were calculated for the experimental results. That is, we use Eqs. (8)–(12), with the only fitted parameters being the apparent diffusivities, $D_1^\dagger$ and $D_2^\dagger$. These fitted curves are also illustrated in Fig. 14.

Figures 15 and 16 show both the experimental and the predicted two-component counterdiffusion results for Sample A (at 65°C). There is good agreement between experiment and theory in most of the diffu-

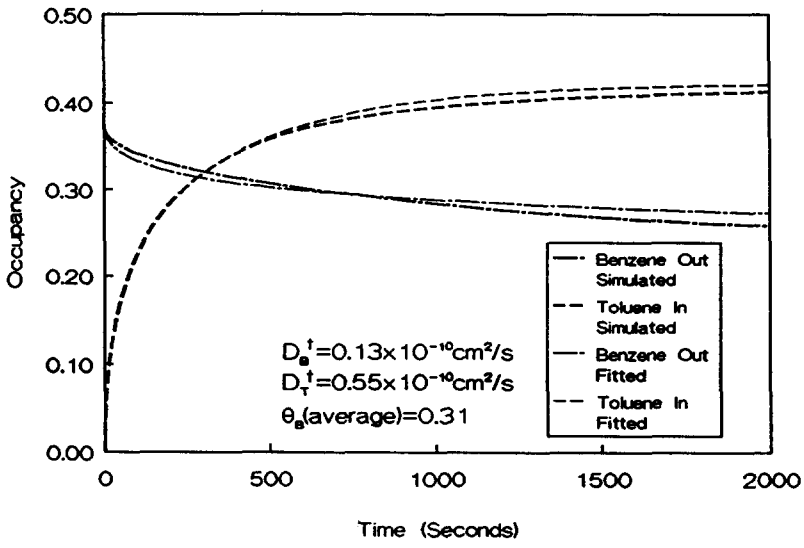

FIG. 14. Example of calculation of theoretical apparent diffusivities for Sample A.

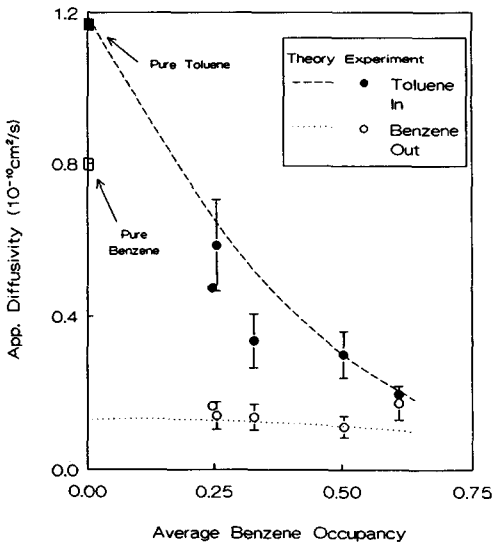

FIG. 15. Experimental and theoretical results for toluene in, benzene out counterdiffusion in Sample A.

sion trends with occupancy, as well as in the magnitude of the predicted reduction in diffusivity caused by the counterdiffusion system. The "pure benzene" and "pure toluene" points in Figs. 15 and 16 correspond to the one-component input parameters that were used in the two-component simulations.

The decreasing trend in the diffusivity of the component coming in is caused by the increasingly tortuous path it has to follow, as the concentration of the presorbed component is increased. The presorbed component displays a much more highly reduced apparent diffusivity. This occurs because, under the conditions of the experiment, the presorbed component faces an incoming front of the adsorbing component resulting in the apparent diffusion coefficient of the first component being greatly reduced. The large reduction in apparent diffusivity of the presorbed component can also be interpreted in terms of the relative concentration gradients of the diffusing components. The presorbed component has a low concentration gradient which is opposed by the large concentration gradient of the adsorbing component. This results in the apparent diffusivity of the presorbed component being greatly reduced, as has been discussed by Qureshi and Wei (2).

At toluene occupancies above 0.6, for the benzene in, toluene out case, a significant increase in the toluene apparent diffusivity was observed. We believe that this was an artifact caused by toluene desorbing off the surface of the crystals, and so that data is not reported here. A small amount of toluene may have condensed on the surface of the crystals at the high toluene partial pressures that are required to obtain occupancies above 0.6. This toluene desorbs quickly when the benzene is injected, resulting in an increase in the measured toluene diffusivity. This behavior did not occur at all with Sample B where a ZSM-5 sample with smoother and cleaner surfaces was used—the rougher surfaces of Sample A probably promote surface condensation to a greater extent. The effect also did not occur with Sample A when the benzene, which condenses less easily than toluene, was at high partial pressure.

The extent of the interaction between the two components can most easily be seen in the concentration profiles of Figs. 17 and

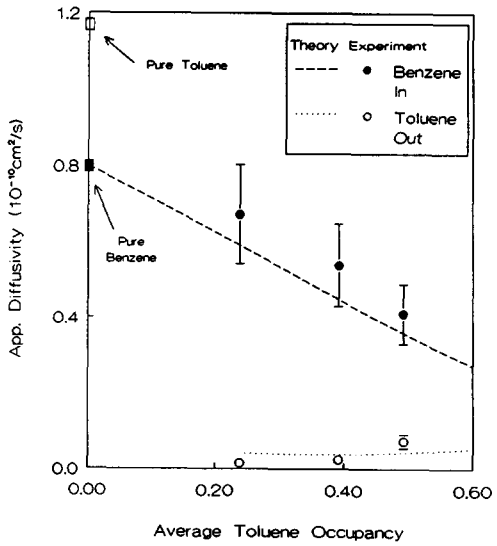

FIG. 16. Experimental and theoretical results for benzene in, toluene out counterdiffusion in Sample A.

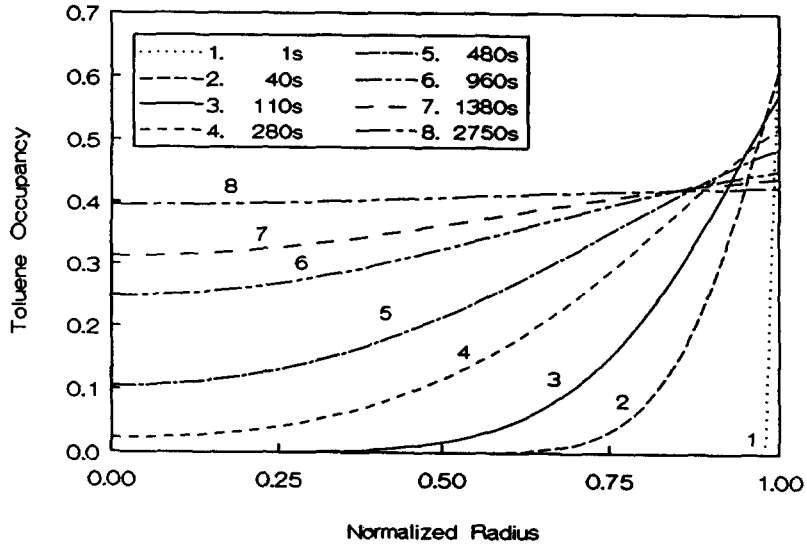

FIG. 17. Toluene occupancy profiles for toluene in, benzene out counterdiffusion (Sample A).

18. These profiles are for the simulated case of initial benzene occupancy equal to 0.375 with toluene injected into the system. The profiles are shown at 1, 40, 110, 280, 480, 960, 1380, and 2750 s after the injection is made. The normalized radius on the abscissa goes from 0 at the center of the particle to 1 at the surface. Thus, Fig. 17 shows the toluene sweeping in, and Fig. 18 shows the benzene being forced out. The most interesting observation is that, as shown in Fig. 18, the concentration of the presorbed benzene can actually be pushed higher than its original concentration at some points inside the catalyst by the driving force of the toluene coming in. At some points inside

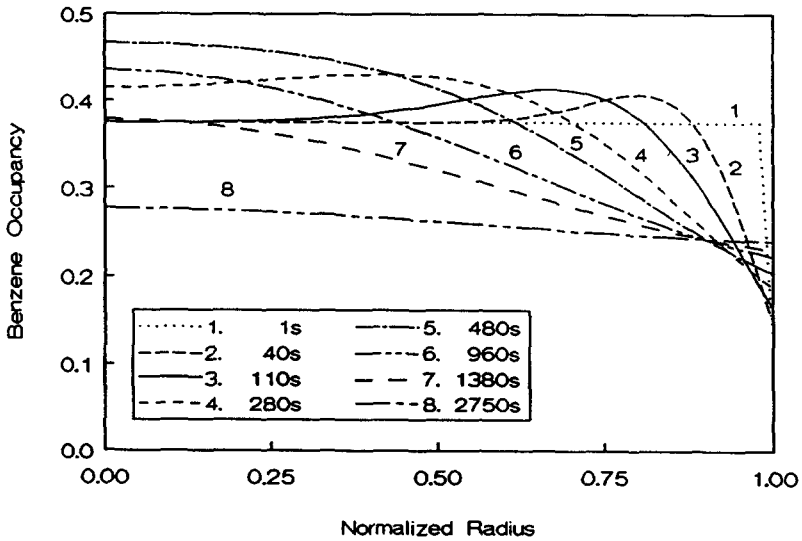

FIG. 18. Benzene occupancy profiles for toluene in, benzene out counterdiffusion (Sample A).

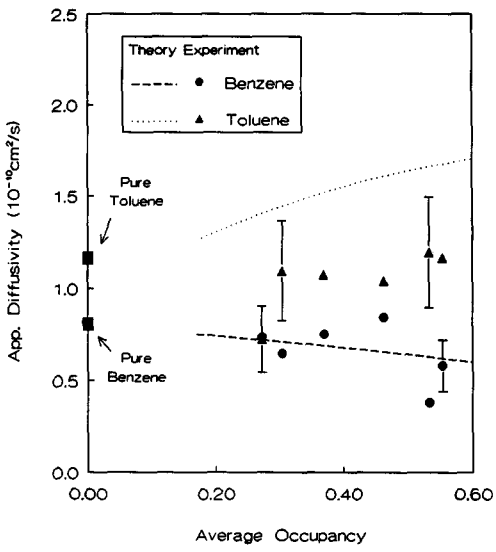

FIG. 19. Experimental and theoretical results for codiffusion of benzene and toluene in Sample A.

the catalyst, the benzene is being forced to diffuse against its own concentration gradient by incoming toluene molecules; that is, entrainment is taking place.

The simplest conclusion of our counterdiffusion results is that there is a decrease in apparent diffusivity compared to the one-component results. This is in agreement with the result of Riekert (*24*), who studied ethane and carbon dioxide in zeolite HT, Ma and Roux (*25*), who studied sulfur dioxide and carbon dioxide in sodium mordenite, and Satterfield and Katzer (*31*) and Satterfield and Cheng (*32*), who studied hydrocarbons in Y type zeolites.

Figure 19 shows codiffusion experimental results for benzene and toluene in Sample A, together with the theoretical predictions (at 65°C). The most significant result here is that the experimental diffusivities do not show large decreases below one-component diffusivities, in contrast to the counterdiffusion results. The codiffusion toluene results lie in the range 1 to 1.2 $\times$ 10^{-10} cm^2 s^{-1}, and the benzene results are of the order of 0.5 to 0.8 $\times$ 10^{-10} cm^2 s^{-1}. These ranges are similar to the ranges covered by the one-component diffusion results shown in Fig. 11. This similarity, between one-component and codiffusion results may have been intuitively expected, since both components are moving in the same direction, and so contrary to the counterdiffusion case, there is not as much interaction between the molecules.

There is qualitative agreement between the model and the experimental results on several points:

1. Both the results predicted by the model (using the one-component parameters, which lie in the range of the one-component data), and the experimental codiffusion results show that toluene should have an apparent diffusivity higher than benzene.

2. Both the model and the experiment indicate that the apparent diffusivities should lie in a range similar to the one-component diffusivities.

3. Both sets of results indicate that there should not be much variation of diffusivity with occupancy. The model predicts that at an occupancy of 0.6, the toluene should appear to diffuse about 45% faster than the one-component diffusivity, and the benzene about 20% slower. This is in contrast to the counterdiffusion predictions where at 0.6 occupancy of the presorbed component, for the toluene in, benzene out case (Fig. 15), the model predicted a factor of 5 decrease for the toluene going in, and a factor of 7 decrease for the benzene coming out. In the case of counterdiffusion for benzene in, toluene out (Fig. 16), the model predicted a factor of 3 decrease for the benzene going in, and a factor of 20 decrease for the toluene coming out.

There is reasonably good quantitative agreement with the model for the benzene codiffusing into the catalyst. However, for the toluene going in, the predicted results are about 30% higher than the experimental results, and show an increasing trend. This increasing trend reflects the models' prediction that there should be some entrainment of the toluene by the benzene, resulting in a

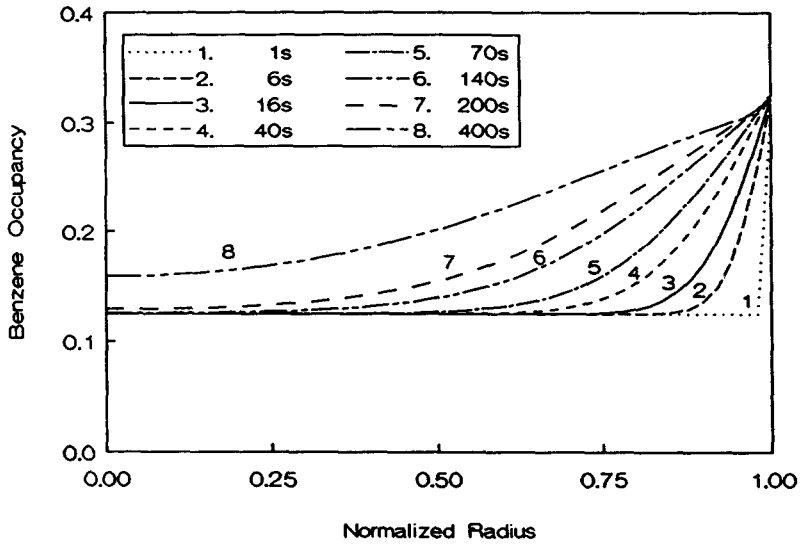

FIG. 20. Benzene occupancy profiles for codiffusion (Sample A).

somewhat increased toluene diffusivity, with the benzene apparent diffusivity being reduced at the same time. Experimentally we do seem to observe this slight reduction in benzene diffusivity; however, there is not as much entrainment of toluene observed as predicted.

Figures 20 and 21 give some insight into why the model predicts that for codiffusion there is some entrainment of the toluene by the benzene. The figures show concentration profiles of benzene and toluene, at eight successive times after injection, when the starting occupancies of benzene and toluene are both equal to 0.125.

To interpret Figs. 20 and 21, it is impor-

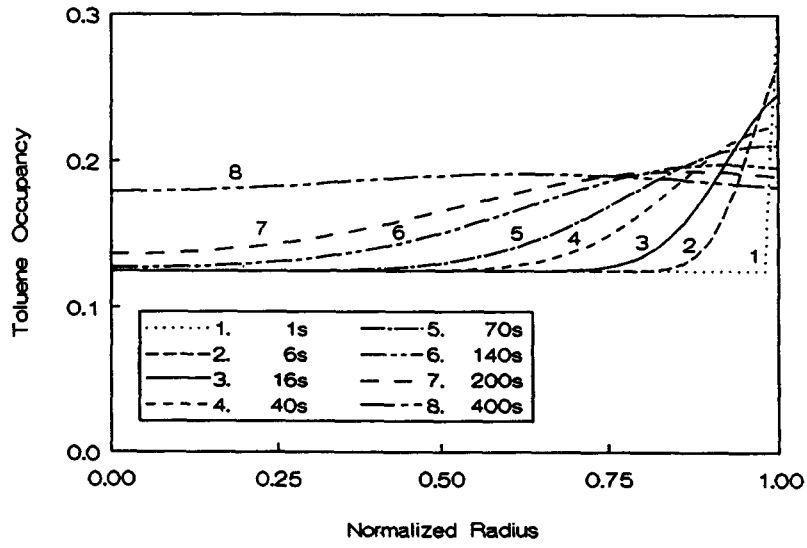

FIG. 21. Toluene occupancy profiles for codiffusion (Sample A).

tant to remember exactly how the codiffusion experiments and simulations were performed.

The first step was to load the catalyst with benzene and toluene, so that at equilibrium the occupancies of benzene and toluene would be equal. This means that the initial gas phase concentration of benzene was much larger than toluene (by about a factor of 4) because benzene is adsorbed less strongly.

The next step was to inject into the gas phase a mixture of benzene and toluene, where the ratio of benzene and toluene in the injected mixture was the same as the ratio in the gas phase. This means that more benzene than toluene is injected (by about a factor of 4). Both components diffuse into the catalyst, but toluene is adsorbed more strongly, and there is less of it present in the gas phase. The result is that the toluene concentration in the gas phase drops rapidly, with the benzene concentration dropping more slowly. Thus, as shown in Fig. 20, the benzene occupancy near the surface of the catalyst remains high, and there is a large occupancy gradient of benzene in the catalyst sustained for a long time. The figure shows that 400 s after injection there is still a substantial benzene occupancy gradient, and the benzene occupancy has not fallen significantly at the surface. In contrast, Fig. 21 shows that the toluene concentration at the surface drops rapidly, as does the toluene concentration gradient near the surface.

Now, in the single-file diffusion model, driving forces are shared. Thus, the benzene concentration gradient drives not only the benzene, but also the toluene, and vice versa. However, the benzene gradient is larger, and is sustained for a longer period of time, and so the toluene benefits from this more than the benzene benefits from the toluene concentration gradient. The result is that the toluene's apparent diffusivity is predicted to be enhanced, at the expense of the benzene's apparent diffusivity.

Two-component diffusion experiments were also performed on Sample B (at 65°C) and the experimental apparent diffusivities compared with the theoretical apparent diffusivities.

Figure 22 shows the case of toluene diffusing in as benzene diffuses out for Sample B. The experimental apparent diffusivity of the toluene going in decreases as a function of the occupancy of the benzene which had been presorbed. The benzene diffusing out displays an apparent diffusivity lower than the toluene coming in.

Figure 23 shows the results for the reverse case, that is, benzene diffusing in, as toluene diffuses out. Once again, the apparent diffusivity of the component going in decreases with the occupancy of the presorbed component, and the presorbed component displays a much reduced apparent diffusivity.

Figures 22 and 23 also show the theoretical predictions. These are based upon the one-component parameters $\alpha^2 q_B = 2.3 \times 10^{-10}$ cm^2 s^{-1} and $\alpha^2 q_T = 3.35 \times 10^{-10}$ cm^2 s^{-1}. In both of these figures the theoretical

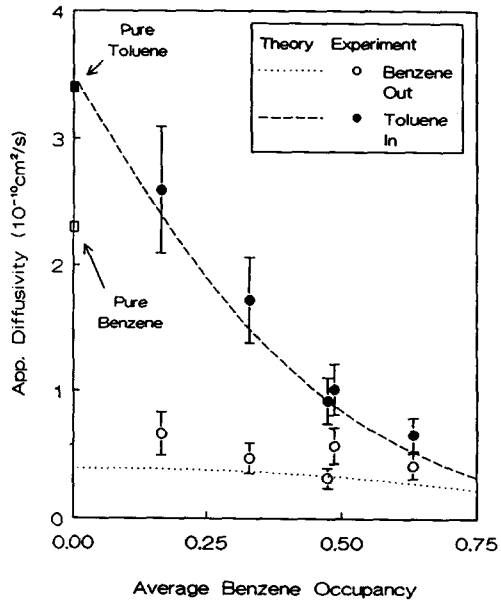

FIG. 22. Experimental and theoretical results for toluene in, benzene out counterdiffusion in Sample B.

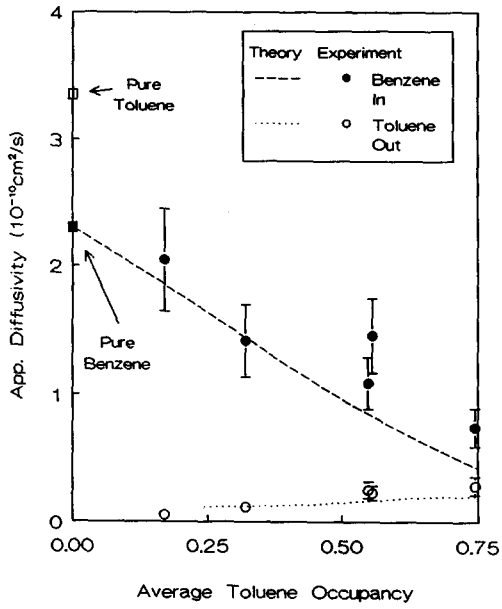

FIG. 23. Experimental and theoretical results for benzene in, toluene out counterdiffusion in Sample B.

predictions are often in quantitative agreement with the experimental results, and, in any case, the trends are in good agreement. These trends are also in good agreement with those obtained on Sample A. See Figs. 15 and 16.

Codiffusion results for Sample B (at 65°C) are shown in Fig. 24. Comparison with Fig. 12 indicates that these results are similar to the one-component diffusion results. The experimental results are somewhat scattered; however, there is not a large reduction of diffusivity with occupancy as was observed with the counterdiffusion results.

The single-file diffusion model predicts that the benzene should entrain the toluene, resulting in the diffusivity of the toluene exhibiting a slightly increasing trend, and the diffusivity of the benzene exhibiting a slightly decreasing trend. Since, the theory for this codiffusion case predicts relatively small changes in apparent diffusion coefficient, it requires very highly precise experiments for comparison. The scatter in our experimental data precludes such a quantitative comparison, but we can claim qualitative agreement on codiffusion conditions giving apparent diffusivities similar to one-component diffusivities, and there being relatively little effect of occupancy on codiffusion.

The important point to note is that all of the two-component experimental diffusion results for Sample B show trends that are very similar to the trends observed earlier on Sample A. In both catalysts the theoretical model gives at least a qualitative description of the experimental results, and sometimes even a quantitative description.

Table 3 summarizes the comparison between Samples A and B, with the third column showing the ratio of each quantity. In the table, K_B and K_T are the two-component Langmuir adsorption constants, D_B and D_T are the one-component diffusion coefficients for benzene and toluene, and $D_B^\dagger$ and $D_T^\dagger$ are the two-component apparent diffusivities of benzene and toluene. All of the above parameters were measured at 65°C. Samples A and B are from different sources, have dissimilar morphologies, and

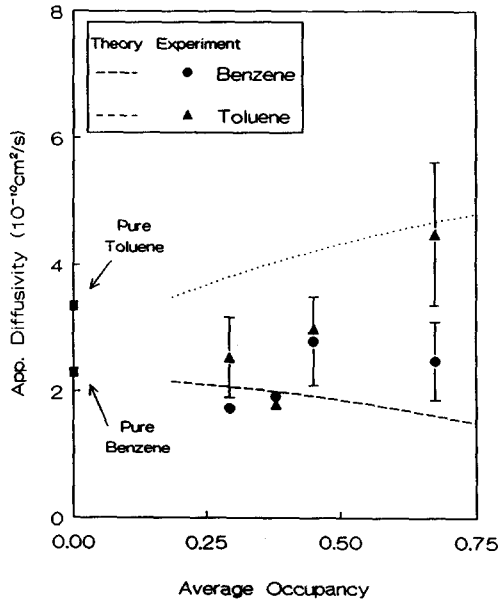

FIG. 24. Experimental and theoretical results for codiffusion of benzene and toluene in Sample B.

TABLE 3

Properties of Samples A and B—Comparison of Morphology, Aluminum Content, Equilibrium Behavior, and Diffusion Results

	Sample A	Sample B	Ratio (B/A)
Source	Peter A. Jacobs	This work	
Morphology	Spheroidal	Hexagonal, twinned	
Size (μm)	12	12 × 20 × 30	
Si/Al ratio	110	6000	50
Isotherm	Langmuir	Langmuir	
Eq. constants[a]	$K_B = 0.025$	$K_B = 0.027$	1
	$K_T = 0.11$	$K_T = 0.11$	1
One-component diffusion[b]	$D_B = 0.7$	$D_B = 2$	3
	$D_T = 1.5$	$D_T = 4$	3
Counterdiffusion[c]			
Toluene in, benzene out	$D_B^{\dagger} = 0.1$	$D_B^{\dagger} = 0.4$	4
	$D_T^{\dagger} = 0.3$	$D_T^{\dagger} = 0.9$	3
Benzene in, toluene out	$D_B^{\dagger} = 0.4$	$D_B^{\dagger} = 1.3$	3
	$D_T^{\dagger} = 0.07$	$D_T^{\dagger} = 0.2$	3
Codiffusion[d]	$D_B^{\dagger} = 0.6$	$D_B^{\dagger} = 2$	3
	$D_T^{\dagger} = 1.1$	$D_T^{\dagger} = 3$	3

[a] Equilibrium constants for the two-component Langmuir Isotherms from Figs. 7 and 8 (Pa^{-1}).
[b] At 0.5 molecules per intersection (10^{-10} cm^2 s^{-1}).
[c] At 0.5 molecules per intersection of presorbed component (10^{-10} cm^2 s^{-1}).
[d] At 0.5 molecules per intersection total occupancy (10^{-10} cm^2 s^{-1}).

Si/Al ratios that differ by a factor of 50. However, the adsorption behavior is essentially identical.

An interesting result is that all of the diffusivities (one-component, counterdiffusion, and codiffusion) are about a factor of 3 higher in Sample B. A factor of 3 is, in of itself, not very remarkable—as mentioned earlier, reported diffusivities in ZSM-5 cover a large range (Table 1); the important point is that all of the diffusivities scale in the same manner, confirming that the diffusion trends in the two samples are very similar.

CONCLUSIONS

A multicomponent diffusion apparatus has been designed and built. It was used to collect data on the diffusion and sorption of benzene and toluene in zeolite ZSM-5. A model based on the single-file diffusion of a lattice gas was used to make predictions of the apparent diffusion coefficients under conditions of counter- and codiffusion. The input parameters for the model were the one-component diffusivities, which were chosen to lie within the range of the experimental one-component results.

There are three major new results:

1. Counterdiffusion and codiffusion experimental results have been obtained on two samples of ZSM-5, in a systematic manner, to investigate occupancy effects of the components.
2. A direct and satisfactory comparison has been made between the experimental counter- and codiffusion results, and a theoretical model of single-file diffusion.
3. Despite different morphologies and Si/Al ratios, all of the experimentally determined diffusion trends for the high silica material (Sample B) agreed well with the trends found for the lower silica material (Sample A), with all of the diffusion coefficients (one-component, counterdiffusion, and codiffusion) scaling in the same manner.

The diffusion trends common to both materials are:

• There is not much effect of occupancy on one-component diffusion.

• For two-component counterdiffusion the component going in displays a decreasing trend, and the component coming out has a very low diffusivity.

• For two-component codiffusion the apparent diffusivities are similar to the one-component diffusivities.

Under counterdiffusion conditions, the decrease of the apparent diffusivity of the component going in could be as much as a factor of 6 when the occupancy of the presorbed component was 0.6. The component coming out displayed a very low diffusivity (up to a factor of about 10 lower than one-component diffusion), and a relatively flat trend. There was good agreement between the trends for the experimental and theoretical results, even to the extent that the model predicted a lower apparent diffusivity for the toluene coming out, than for the benzene coming out.

For codiffusion, both components displayed apparent diffusivities that were relatively independent of occupancy, and of similar magnitude as the one-component diffusion coefficients. There is qualitative agreement between the experimental and theoretical codiffusion results in terms of toluene diffusing faster than benzene, the diffusivities lying in a range similar to one-component diffusivities, and there being not much variation of diffusivity with occupancy.

The experimental data of one-component diffusion showed no dramatic effect of occupancy up to an occupancy of about 0.75. Toluene had a diffusivity in the range of 1 to 2×10^{-10} cm^2 s^{-1} and benzene in the range 0.6 to 0.9 $\times 10^{-10}$ cm^2 s^{-1} at 65°C for Sample A. The corresponding ranges for Sample B were 2 to 4 $\times 10^{-10}$ cm^2 s^{-1} for toluene and 1.3 to 2.5 $\times 10^{-10}$ cm^2 s^{-1} for benzene.

The model predicts isotherms of the Langmuir form for both one- and two-component systems. It was found that these isotherms were a good approximation to both the one- and two-component experimental results at 65°C. No significant differences in adsorption behavior were found for the two zeolites, which was not an unexpected result since both materials have low absolute quantities of aluminum.

The similar adsorption behavior and diffusion trends of Samples A and B indicated that the internal structure of the two materials is in many ways alike, and the interactions between the diffusing molecules for both one- and two-component diffusion are the same for the two samples.

APPENDIX: NOMENCLATURE

Variables

$\mathbf{D}$	Constitutive diffusion matrix
$\mathbf{D}^{\dagger}$	Apparent diffusivity matrix
D	One-component diffusivity (cm^2 s^{-1})
$D_i^{\dagger}$	Apparent diffusivity of component i (cm^2 s^{-1})
K	Langmuir Isotherm constant (Pa^{-1})
m	Mass of crystals (g)
P	Partial pressure (Pa)
P_{sat}	Saturated vapor pressure (Pa)
q	Hopping rate of a molecule to a specific adjacent site, in an otherwise empty lattice (s^{-1})
q_i	Hopping rate of a molecule of the ith component to a specific adjacent site, in an otherwise empty lattice (s^{-1})
R	Crystal radius (cm)
R_g	Gas–law constant (Pa cm^3 mol^{-1} K^{-1})
r	Radial coordinate (cm)
T	Temperature (K)
t	Time coordinate (s)
V_g	Gas phase volume (cm^3)

Greek

α	Distance between grid intersections (cm)
$\underline{\theta}$	Occupancy vector
$\bar{\theta}$	Volumetric average occupancy (molecules/intersection)
θ_i	Occupancy of component i (molecules/intersection)
θ	Occupancy in one-component system (molecules/intersection)
ρ	Moles of intersections per gram of catalyst (mol g^{-1})

Subscripts

B Benzene
i ith component
i_0 Initial condition for ith component
0 Initial condition in one-component system
T Toluene

Superscripts

† Apparent diffusivity or apparent diffusivity matrix

ACKNOWLEDGMENTS

We are grateful to Dr. Peter A. Jacobs of The Katholieke Universiteit Leuven, Belgium for supplying us with the ZSM-5 sample used in this study. We thank Dr. Roland von Ballmoos for the helpful discussions on the synthesis of ZSM-5, and Carlonda L. Russell for performing much of the synthesis work.

REFERENCES

1. Derouane, E. G., *in* "Catalysis on the Energy Scene" (S. Kaliaguine and A. Mahay, Eds.), p. 1. Elsevier, Amsterdam, 1984.
2. Qureshi, W. R., and Wei, J., *J. Catal.* **126,** 126 (1990).
3. Shah, D. B., Hayhurst, D. T., Evanina, G., and Guo, C. J., *AIChE J.* **34,** 1713 (1988).
4. Zikanova, A., Bülow, M., and Schlodder, H., *Zeolites* **7,** 115 (1987).
5. Bülow, M., Schlodder, H., Rees, L. V. C., and Richards, R. E. *in* "Proceedings of the Seventh International Zeolite Conference" (Y. Murakami, A. Iijima, and J. W. Ward, Eds.), p. 579. Elsevier, Amsterdam, 1986.
6. Tsikoyiannis, J. G., Ph.D. thesis, Massachusetts Institute of Technology, 1986.
7. Prinz, D., and Riekert, L., *Ber. Bunsen ges. Phys. Chem.* **90,** 413 (1986).
8. Nayak, V. S., and Riekert, L., *in* "Proceedings of the International Symposium on Zeolite Catalysis" p. 157. Siofok, Hungary, 1985.
9. Le Van Mao, R., Ragaini, V., Leofanti, G., and Fois, R., *J. Catal.* **81,** 418 (1983).
10. Heering, J., Kotter, M., and Riekert, L., *Chem. Eng. Sci.* **37,** 581 (1982).
11. Wu, P., Debebe, A., and Ma, Y. H., *Zeolites* **3,** 118 (1983).
12. Doelle, H.-J., Heering, J., and Riekert, L., *J. Catal.* **71,** 27 (1981).
13. Olson, D. H., Kokotailo, G. T., and Lawton, S. L., *J. Phys. Chem.* **85,** 2238 (1981).
14. Forni, L., Viscardi, C. F., and Oliva, C., *J. Catal.* **97,** 469 (1986).
15. Chiang, A. S., Dixon, A. G., and Ma, Y. H., *Chem. Eng. Sci.* **39,** 1451 (1984).
16. Hayhurst, D. T., and Paravar, A. R., *Zeolites* **8,** 27 (1988).
17. Ma, Y. H., and Savage, L. A., *AIChE J.* **33,** 1233 (1987).
18. Haag, W. O., Lago, R. M., and Weisz, P. B., *Faraday Discuss. Chem. Soc.* **72,** 317 (1981).
19. Caro, J., Stanko, H., Kärger, J., and Riekert, L., *Zeolites* **6,** 213 (1986).
20. Lechert, H., Wienecke, J., and Basler, W. D., *in* "Proceedings of the International Symposium on Zeolite Catalysis," p. 147. Siofok, Hungary, 1985.
21. Choudhary, V. R., and Srinivasan, K. R., *J. Catal.* **102,** 328 (1986).
22. Eic, M., and Ruthven, D. M., *in* "Zeolites: Facts, Figures, Future" (P. A. Jacobs and R. A. van Santen, Eds.), p. 897. Elsevier, Amsterdam, 1989.
23. Habgood, H. W., *Canad. J. Chem.* **36,** 1384 (1958).
24. Riekert, L., *AIChE J.* **17,** 446 (1971).
25. Ma, Y. H., and Roux, A. J., *AIChE J.* **19,** 1055 (1973).
26. Kärger, J., and Bülow, M., *Chem. Eng. Sci.* **30,** 893 (1975).
27. Ma, Y. H., and Lee, T. Y., *Ind. Eng. Chem. Fundam.* **16,** 44 (1977).
28. Ruthven, D. M., and Kumar, R., *Canad. J. Chem. Eng.* **57,** 342 (1979).
29. Kumar, R., Duncan, C., and Ruthven, D. M., *Canad. J. Chem. Eng.* **60,** 493 (1982).
30. Yasuda, Y., and Matsumoto, K., *J. Phys. Chem.* **93,** 3195 (1989).
31. Satterfield, C. N., and Katzer, J. R., *Adv. Chem. Ser.* **102,** 193 (1971).
32. Satterfield, C. N., and Cheng, C. S., *AIChE J.* **18,** 724 (1972).
33. Förste, C., Germanus, A., Kärger, J., Pfeifer, H., Caro, J., Pilz, W., and Zikanova, A., *J. Chem. Soc. Faraday Trans. 1* **83,** 2301 (1987).
34. Theodorou, D., and Wei, J., *J. Catal.* **83,** 205 (1983).
35. Kärger, J., Pfeifer, H., Caro, J., Bülow, M., Schlodder, H., Mostowicz, R., and Völter, J., *Appl. Catal.* **29,** 21 (1987).
36. Mo, W.-T., Ph.D. thesis, Massachusetts Institute of Technology, 1988.
37. Choudhary, V. R., Akolekar, D. B., and Singh, A. P., *Chem. Eng. Sci.* **44,** 1047 (1989).
38. Post, M. F. M., van Amstel, J., and Kouwenhoven, H. W., *in* "Proceedings of the Sixth International Zeolite Conference" (D. Olson and A. Bisio, Eds.), p. 517. Butterworths, London, 1984.
39. Lechert, H., and Schweitzer, W., *in* "Proceedings of the Sixth International Zeolite Conference" (D. Olson and A. Bisio, Eds.), p. 210. Butterworths, London, 1984.
40. Wu, P., and Ma, Y. H., *in* "Proceedings of the

Sixth International Zeolite Conference" (D. Olson and A. Bisio, Eds.), p. 251. Butterworths, London, 1984.

41. von Ballmoos, R., "Collection of Simulated XRD Powder Patterns for Zeolites." Butterworths, London, 1984.
42. von Ballmoos, R., "The ^{18}O-Exchange Method in Zeolite Chemistry." Salle und Sauerländer, Frankfurt am Main, 1981.
43. Qureshi, W. R., Ph.D. thesis, Massachusetts Institute of Technology, 1989.
44. Walker, J. Q., Jackson Jr., M. T., Maynard, J. B., "Chromatographic Systems." 2nd Ed., pp. 321–325. Academic Press, New York, 1977.
45. Powell, M. J. D., *Comput. J.* **7,** 303 (1965).
46. Kuester, J. L., and Mize, J. H., "Optimization Techniques with Fortran." p. 251. McGraw–Hill, New York, 1973.